Powder Technology 262 (2014) 249–256

Contents lists available at ScienceDirect

Powder Technology

journal homepage: www.elsevier.com/locate/powtec

Collapse of a granular column under rotation

J.M. Warnett [a,*], P. Denissenko [a], P.J. Thomas [a], M.A. Williams [b]

[a] School of Engineering, University of Warwick, Gibbet Hill Road, Coventry CV4 7AL, UK
[b] Warwick Manufacturing Group, University of Warwick, Gibbet Hill Road, Coventry CV4 7AL, UK

ARTICLE INFO

Article history:
Received 30 August 2013
Received in revised form 9 March 2014
Accepted 5 April 2014
Available online 16 April 2014

Keywords:
Granular collapse
Rotational collapse
Avalanches

ABSTRACT

Experimental results for the collapse of granular columns on a rotating table are presented. In the non-rotating case two flow regimes are exhibited dependent on the aspect ratio $a = h_0/r_0$, where h_0 is the initial height and r_0 is the initial column radius. Scaling relations for the characteristic geometrical properties of the collapsed column under varying rotation rates are obtained. As the rotation rate increases, material is lost from the main pile and travels to the edge of the rotating table. This results in a decrease in the final radius of the main collapsed pile, as material is lost during this secondary, rotation-induced spreading phase. The degree of mass ejection in the secondary spread increases with rotation frequency for a given initial aspect ratio. Analysis of the flow characteristics including time evolution and final pile height are also described.

1. Introduction

The study of granular flows is important to gaining an understanding of environmental particulate movements. Insight into natural deluges such as avalanches and pyroclastic flows and sediment transport processes has been developed through experimental, theoretical and numerical studies of idealised granular flows [1–4]. Many industrial processes involve the transportation of grains and powders, which can be optimised with improved understanding of the underlying granular dynamics.

Static granular flows are important to civil engineering projects, predominantly in the storage of grains and powders in silos and geotechnical retaining walls. Failure of these containers is analogous to a 'dam break' investigated by several previous authors [5,6]. A description of these flows has been offered by interpretation of experiments on the collapse of a granular column [7–11] and the failure of a granular step [5,12–16]. The simplified geometry provides data with traceable boundary conditions for testing theories, thus linking the theoretical models with the dam break itself.

An agricultural application where granular flows are utilised is the distribution of fertilisers and seeds. This is achieved by a continuous injection of granular material via a hopper, which falls onto a centrifuging disc of a prescribed frequency to ensure the even spreading of the material. This has been a recent subject of investigation, both experimentally and computationally [17–20].

Granular flows display properties of a solid (stationary), liquid (avalanching flows) and a gas (saltation of grains), often simultaneously as in the case of granular column collapse. Theoretical models of this arrangement derived from hydrodynamic approximations [2,21–24], while on the whole describe the flow regime well, can occasionally diverge from the true flow precisely due to this nature when verified against experimental results. Any model which extends this case to include rotation requires similar experimental data to validate the theoretical framework given its potential to deviate from reality.

The current investigation incorporates rotation with the collapse of a granular column. A cylinder filled with granular material was placed centrally on a rotating table of prescribed frequency. The cylinder was then quickly removed and the resulting flow observed. The granular column slumped to form a pile similar to the non-rotating case, but rotation caused mass to continue to be extruded from this pile in a secondary rotation-induced spreading regime. The purpose of this study is to discover how rotation frequency affects the scaling laws describing the pile for non-rotating granular column collapse as expressed by previous authors [7–9], and to find the onset and degree of granular spreading. Some parallels can be drawn with the arrangements for spreading of seeds and fertilisers, but is still more akin to a dam break situation. The derived empirical relations could find future application in the testing of new granular rheologies in different flow regimes.

A description of the experimental procedure is given in Section 2. Qualitative investigations into collapse dynamics are detailed in Section 3. Results on the relations between experimental parameters are presented in Section 4. Scaling laws are given for final runout and height and how these parameters advance with time, found to be dependent upon the initial column setup and the frequency of the rotating table. When the rotation rate is high enough the secondary rotation-induced spreading regime envelopes leading to material ejection which is described and quantified. Discussion and an overview of this research are presented in Section 5.

* Corresponding author at: University of Warwick, Coventry, UK. Tel.: +44 7736949639.
E-mail address: j.m.warnett@warwick.ac.uk (J.M. Warnett).

http://dx.doi.org/10.1016/j.powtec.2014.04.030
0032-5910/

2. Experimental setup

2.1. Apparatus

A cylinder of radius r_0 was aligned centrally on a rotating turntable and filled with granular material to a specified height h_0 as shown in Fig. 1. The table was then set into rotation at a frequency f, and the column of material allowed to enter solid body rotation. The cylinder was mechanically removed vertically via a system of pulleys directly above the tank and the granular material allowed to collapse. Its removal time, $t_r = h_0/v$, is required to be small compared to the time for the mass to be set into motion, approximately calculated as $t_m = \sqrt{2h_0/g}$. The average removal speed of $v = 2.5\text{ms}^{-1}$ used was sufficient for this to hold up to the tallest column $h_0 = 63$mm where $t_r = 0.03$s and $t_m = 0.11$s.

Cylinders of inner radius $r_0 = 20$ mm, 25 mm, 30 mm, 36 mm were used. For each cylinder radius, the initial height of the column of granular material, h_0, and frequency, f, were varied systematically. The aspect ratio of the initial column is defined by $a = h_0/r_0$, determined by the initial mass of granular material m_0. The aspect ratio was varied in the range 0.28–1.75, and frequency in the range 0.0–1.7 Hz.

A calcium carbonate granular material of bulk density ≈ 1.6 g/cm^3 and particle size $d = 0.6$–0.8 mm was used throughout these experiments. The particulate had an internal friction angle $\theta_\mu \approx 39^\circ$ and an angle of repose $\theta_r \approx 30^\circ$. The material was dried in an oven to evaporate any residual moisture, minimising cohesive effects between particles. The initial column was prepared by funneling the granular material into the cylinder, and the top was flattened to ensure uniform height of the column, accurate to ± 1 mm. The method of preparation showed good repeatability with a mean packing density, $\phi = m_0/(\pi r_0^2 h_0 \rho)$, between 0.78 and 0.82 across all prepared columns.

2.2. Measurement and accuracy

Time evolution of the resultant flow was studied by recording the collapse within the rotating frame of reference using a high speed digital camera fixed to the spinning table with a frame rate of 240 fps. This enabled data capture of the radial runout as a function of time, $r(t)$, and was also used to determine the collapse duration, t_f. Interpreting the video with image processing software allowed a spatial resolution of 0.5 mm when recording radial values. The resultant accuracy was of the order ± 3 mm due to the uneven periphery observed, increasing to ± 5 mm for the higher frequencies.

After the collapse occurs several dimensional values were measured from the resultant deposit. The final pile radius, r_f, was recorded using an alignment sheet fixed to the surface with radial markings of 10 mm in conjunction with a horizontal vernier scale accurate to ± 0.2 mm. The final height, h_f, was recorded with similar accuracy using a vernier height gauge. In the case where granular material was lost from the main pile and thrown to the edge of the tank the final mass of the resultant pile, m_f, was recorded by sweeping up the granular material, but resulted in some particles being lost in transit. The method was trialled with known masses of granular material, and was found to be accurate to ± 1.5 g.

A known source of error in recording the final pile radius r_f is the uneven periphery. Experiments have shown that in the case of no rotation this is approximately 3–4 particle diameters for the range of aspect ratios trialled, with the effect becoming more pronounced for increased values of rotation reaching up to 6–7 particle diameters. This uncertainty was considered during repeatability testing performed across various aspect ratios and frequencies. If was found that r_f, h_f and m_f varied by ± 3.0 mm, ± 1.0 mm and ± 2.0 g respectively.

3. Collapse dynamics

3.1. Flow description

The collapse in the non-rotating case is well reported by previous authors [7,8]. The collapse begins with the periphery of the column starting to crumble and avalanche. This causes a frontal flow to develop at the foot of the column, which propagates radially outwards eventually defining the final pile radius. Simultaneously there is a discontinuity that separates the frontal flow and the central static summittal region, which propagates inwards and is eventually consumed by the avalanche. The propagation of the discontinuity may continue for a proportionally short phase after the column has ceased to spread, acting only to alter the profile of the deposit which can only sustain material at an angle less than the angle of repose. With the introduction of rotation a second set of dynamics envelopes as can be seen in Fig. 2 and further shown by the video in the journal online.

The avalanching begins in the same way as described above but the rotation of the table actuates a non-zero azimuthal component of the front flow at the foot of the pile as can be seen in Fig. 2. The photos in Fig. 2 are taken from the camera mounted on the tank rotating in an anticlockwise (negative azimuthal) direction. It is observed that, due to Coriolis effects, the particulate moves in a positive azimuthal direction within the rotating frame of reference while flowing radially outwards, resulting in curvature of the runout (for video see supplementary material online). Rotation induces higher avalanche front speeds than in the non-rotating collapse, causing greater radial spread of granular material and results in a faster propagation rate of the discontinuity between central static and avalanching regions. The result is a greater final deposit radius, r_f, up to a given frequency f_{crit}. It appears that as the frequency increases, the discontinuity disappears before the spreading phase is over in contrast to the static case. It is difficult to pinpoint where this occurs given that this profile altering stage was extremely short, even in the static case, but it was observed that after the discontinuity disappears the avalanching flow continues to feed the front until the spreading ceases.

Where f_{crit} is passed for a particular cylinder size and aspect ratio there is a secondary rotation-induced spreading phase as described in Fig. 3. The first stage of the collapse results in the pile spreading to a radius r_{max}. If $f < f_{crit}$ then this radius is exactly r_f. If $f > f_{crit}$ then some material at the edge of the pile is lost and moves to the edge of the table. This rotation-induced spreading phase results in a retraction of the radius of the resultant pile to a value r_{crit} where the process of material ejection ceases and the radius stagnates. This is then the final pile radius r_f. The reason for this is that the centripetal force is great enough to

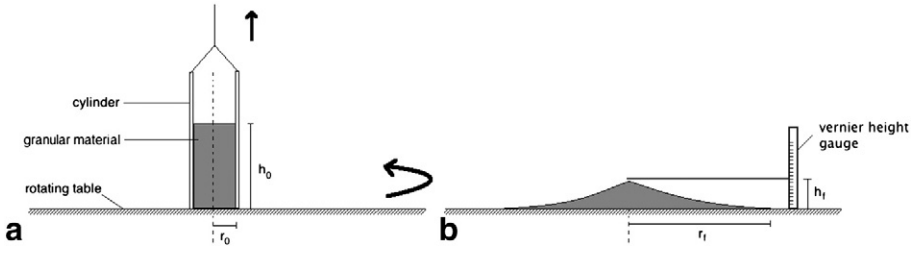

Fig. 1. Experimental setup. **a** Initial setup of granular column on rotating table. **b** After collapse.

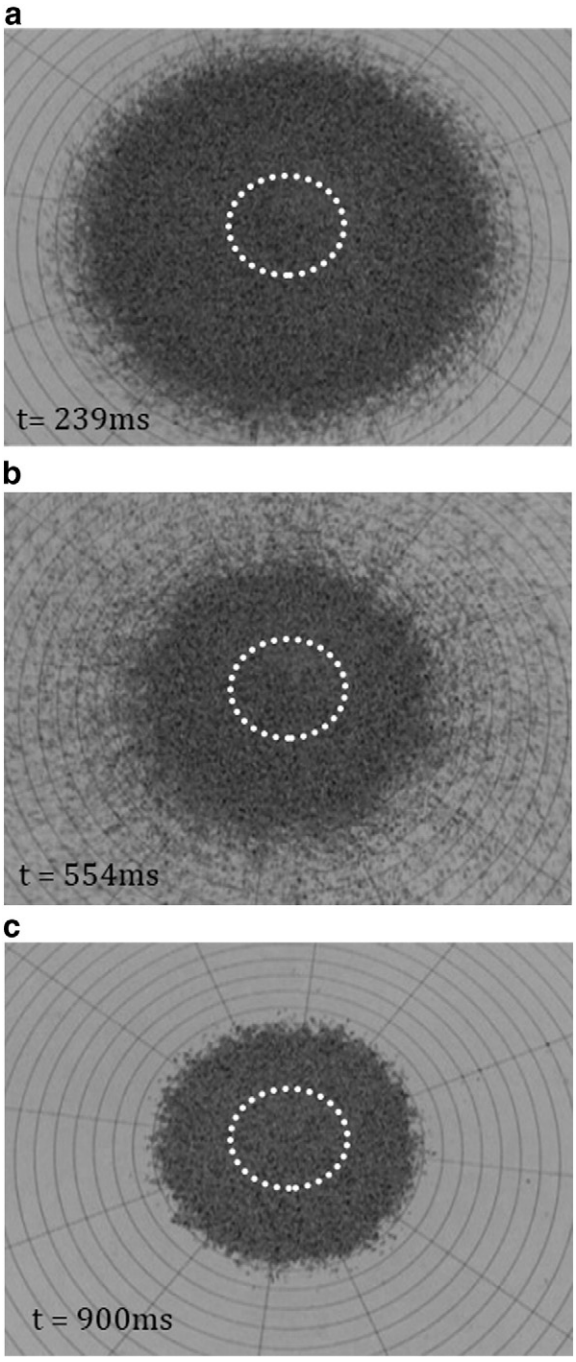

Fig. 2. Collapse of column with $r_0 = 36$ mm, $a = 1.38$, $f = 1.41$ Hz where material leaves the main pile. The white outline marks the initial position of the cylinder. **a** Runout of the pile at its maximum. **b** Material is leaving the main pile and being thrown to the edge of the tank. **c** The final deposit left where no more material is drawn from the main pile.

overcome frictional effects felt by the particles at a specific radius, allowing the continued motion of granular material that overstretches the critical radius. Quantification of this dynamic is given in Section 4.

3.2. Deposit morphology

There are two distinct morphologies that result from the granular collapse dependent upon aspect ratio as shown in Fig. 4; a truncated cone and a full conical shape. The development of the cone has been proposed to be dependent upon the internal friction angle θ_μ by Lajeunesse et al. [8], where the avalanching occurs over an internal cone of radius r_0 and base angle θ_μ.

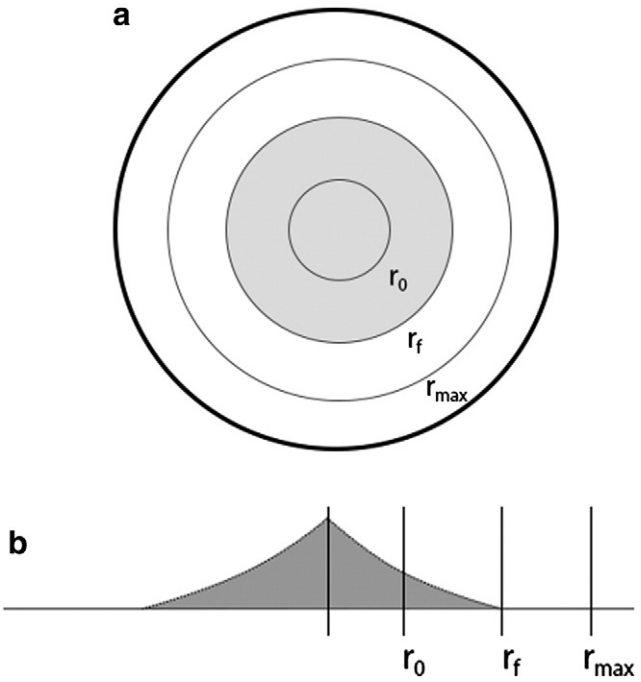

Fig. 3. Dimensions of the rotational collapse showing the initial cylinder radius r_0, the maximal radius r_{crit}, has been passed the final pile radius retracts to r_f. Grey marks the resting place of granular material when all movement has ceased. **a** Top view. **b** Side view.

In the case with no rotation for $a < 0.78$, the summit is never completely consumed by the collapse and results in a truncated cone morphology. Exceeding this aspect ratio, the summit is consumed and results in the full conical shape. This critical aspect ratio is in good agreement with previous research [7–9] where a value of $a = 0.74$ was obtained ($a = 0.90$ in [9]) and will vary dependent upon the value of θ_μ for the particulate. The critical value of $a = 0.78$ obtained in this study is consistent with the interpretation of a failure surface with angle θ_μ given $tan(\theta_\mu) = 0.81$.

With the introduction of rotation, the boundary between the frontal flow and the central static summittal region propagates further inwards than in the case of no rotation. Overall this leads to the earlier

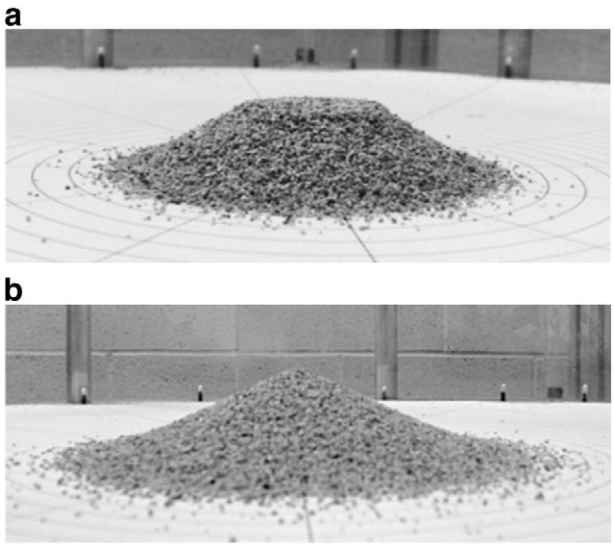

Fig. 4. Different collapse regimes. **a** $r_0 = 36$ mm, $a = 0.60$. Summit not consumed. **b** $r_0 = 36$ mm, $a = 1.20$. Summit consumed leaving a full conical shape.

appearance of the cone shape where the entirety of the summit is consumed. This is due to the effective direction of gravity being tilted by an angle

$$tan\theta = \frac{(2\pi f)^2 r_0}{g} \tag{1}$$

arising from the ratio of centripetal and gravitational forces. A natural non-dimensionalisation of frequency can be given

$$f_* = f\sqrt{\frac{r_0}{g}}, \tag{2}$$

hence

$$tan\theta = (2\pi f_*)^2. \tag{3}$$

Assuming the onset of a full conical shape to be dependent on the angle of internal friction in the case of no rotation, i.e. $a_{cone,f=0} = tan\theta_\mu$, with rotation the onset a_{cone} would be expected to occur at approximately

$$a_{cone} = a_{cone,f=0} - (2\pi f_*)^2. \tag{4}$$

Experimentally achieved data for a_{cone} is plotted against normalised frequency f_* in Fig. 5 revealing the relation

$$a_{cone} = 0.78 - 32.2 f_*^2 \tag{5}$$

in good agreement with the above derivation.

4. Scaling results

4.1. Final radius

Initially the final pile radius against aspect ratio was considered for each frequency. The final radius was normalised

$$r_* = \frac{r_f - r_0}{r_0}. \tag{6}$$

It can be seen in Fig. 6 that for all f the relationship between normalised final radius and aspect ratio is linear up to an aspect ratio a_{crit}, where the final radius stagnates at a value r_{crit} due to the secondary rotation-induced spreading phase. This results in relations of the form

$$\begin{aligned} r_* &= \Lambda a & a < a_{crit} \\ r_* &= \frac{r_{crit} - r_0}{r_0} & a > a_{crit} \end{aligned} \tag{7}$$

where Λ is a frequency dependent constant. Linearity of this relation can be expected from dimensional analysis and has been shown by Lube et al. [7]. Grain size and type, inter-granular friction and surface roughness could also affect the value of Λ but has been discounted in this analysis.

Λ is normalised as

$$\Lambda_* = \frac{\Lambda - \Lambda_0}{\Lambda_0} \tag{8}$$

where Λ_0 is the value of Λ for no rotation, and is compared with f_*^2 in Fig. 7. While the gravitational forces dominate and the centrifugal force is weak, this follows a quadratic order relation in f_*^2. Then as $f_*^2 > 0.0024$ the centrifugal forces begin to have a dominant role on the radial runout and a linear relationship envelopes, calculated to be where the centrifugal forces are approximately 10% of the gravitational force. These relations can be described

$$\begin{aligned} \Lambda_* &= 16700 f_*^4 + 10 f_*^2 & f_* < 0.049 \\ \Lambda_* &= 110 f_*^2 - 0.15 & f_* > 0.049 \end{aligned} \tag{9}$$

A comparison of r_* with frequency for fixed a for $r_0 = 36$ mm is shown in Fig. 8. It is observed that r_* steadily increases with rotation rate until the runout reaches a radius experiencing a centripetal

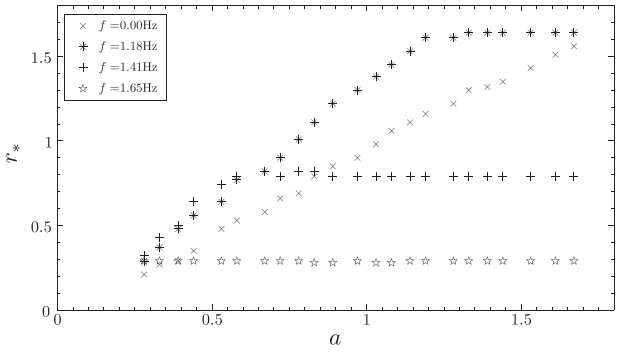

Fig. 6. Normalised final pile radius, r_*, against aspect ratio where $r_0 = 36$ mm for various frequencies showing the eventual stagnation of the radius of the final deposit.

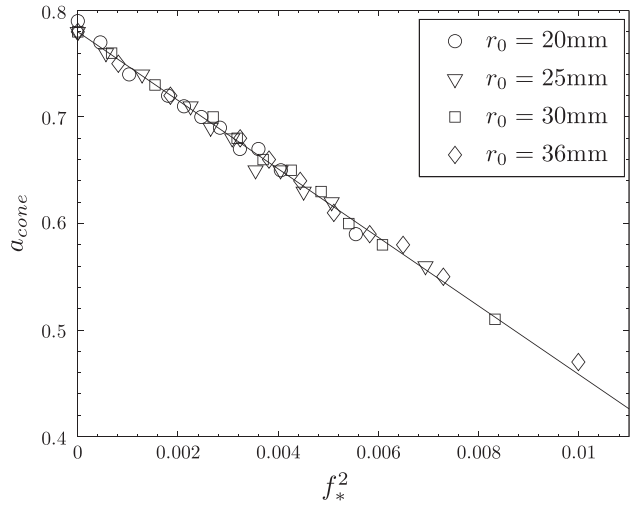

Fig. 5. Dependence of frequency f_* on the onset of the second regime a_{cone}. Line fit as given in Eq. (5).

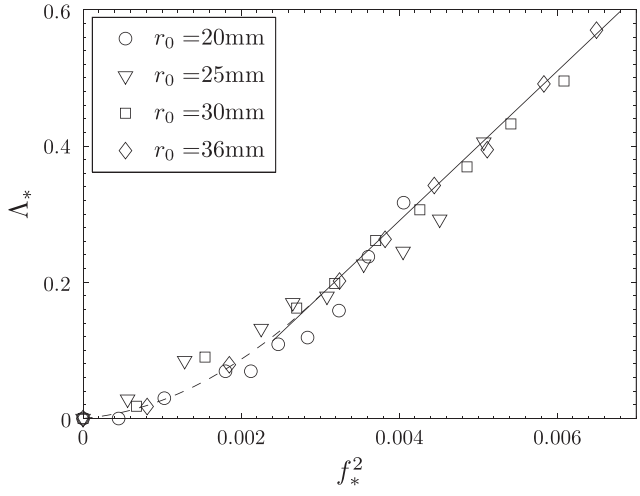

Fig. 7. Increase in the value of Λ_* as f^2_* varies for different cylinder sizes. Initially it follows a quadratic relation shown by (− −), then when $f^2_* > 0.0024$ the relation is linear shown by (−) as described by Eq. (9).

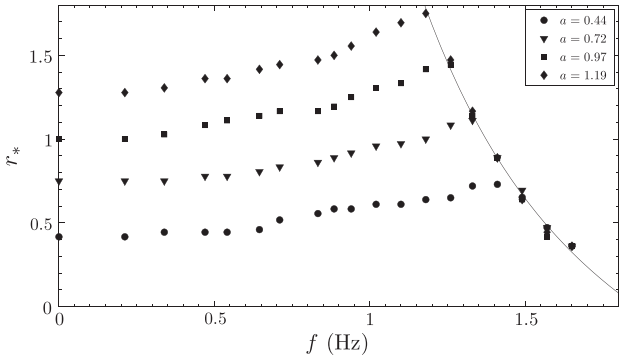

Fig. 8. Normalised final pile radius, r_* against frequency for various aspect ratios where $r_0 = 36$ mm. All cylinder radii followed the same dynamic, settling on the line fit shown given by Eq. (10).

acceleration strong enough to overcome frictional effects at a frequency f_{crit}. It is at this point where the secondary rotation-induced spreading phase begins to occur resulting in mass ejection from the final deposit. Further increases in frequency find that r_* is inversely proportional to f^2, with all aspect ratios falling to the same line.

By considering known values of f_{crit} for stagnating r_f and the centripetal acceleration at this radius it was found that

$$r_{crit}(2\pi f_{crit})^2 = 5.7\text{ms}^{-2} \tag{10}$$

as indicated by the solid line in Fig. 8. It follows that the critical centripetal acceleration where material is lost from the main pile is 5.7 ms^{-2} for this particular setup. At this point the frictional force, $F_f = \mu mg$, and centripetal force, $F_r = mr(2\pi f)^2$, acting on a given particle are equal. By rearrangement of this equivalence the frictional coefficient between the table and granular material can be derived, giving

$$\mu = r_{crit}\frac{(2\pi f_{crit})^2}{g}. \tag{11}$$

Using experimental data found from this setup as in Fig. 8, it is calculated that $\mu = 0.58$. Affirmation of this method of calculation was given by determination of the value of friction using a slope made of perspex as per the table and finding the angle at which the material begins to slide, and was found to be 0.57.

The aspect ratio of the secondary rotation-induced spreading a_{crit} occurs for

$$a_{crit} = \frac{r_{*,crit}}{\Lambda} \tag{12}$$

from Eq. (7) where $r_{*,crit}$ is the normalised critical radius that can be calculated from Eq. (10). Then by applying Eqs. (8) and (9)

$$a_{crit} = \frac{r_{*,crit}}{\Lambda_0(110f_*^2 + 0.85)}. \tag{13}$$

Eqs. (9) and (10) can be substituted into Eq. (7) to give a full description of the final pile radius for known a, Λ_0 and f_*. When $a < a_{crit}$ the normalised final pile radius r_* is given by

$$\begin{aligned} r_* &= a\Lambda_0\left(16700f_*^4 + 10f_*^2 + 1\right) \quad f_* < 0.049 \\ r_* &= a\Lambda_0\left(110f_*^2 + 0.85\right) \quad f_* > 0.049 \end{aligned} \tag{14}$$

and when $a > a_{crit}$ the final pile radius is more simply defined

$$r_* = \frac{5.7\text{ms}^{-2}}{(2\pi f_*)^2 g} - 1. \tag{15}$$

4.2. Final deposit height

The final deposit height h_f is dependent upon the initial height, h_0, aspect ratio a and the frequency of rotation, f.

While the final deposit is a truncated cone observed in Fig. 4, the final height is clearly $h_f = h_0$. Observing the non-dimensionalisation

$$h_* = h_0/r_0 \tag{16}$$

that is to say $h_* = a$. At the onset of the full conical shape where $a = a_{cone}$ the entirety of the summit is consumed by the avalanching of the layers and the inwardly propagating boundary between the frontal flow and static region. Continuing to increase a results in $h_f < h_0$ and a rapid stagnation of h_* occuring at an aspect ratio a_h dependent on frequency. For increasing $a > a_{cone}$, the summit experiences a decrease in curvature before the existence of a sharp peak where h_f ceases to grow with aspect ratio. Due to this transitional period a_h is found to occur at a slightly higher aspect ratio than the onset of the second regime a_{cone} as noted by Lube et al. [7].

As the rotation rate increases the value of a_h decreases shown in Fig. 9, also demonstrates independence of r_0. This results in the relation

$$h_* = a \quad a < a_h \tag{17}$$

$$h_* = a_h \quad a > a_h \tag{18}$$

where

$$a_h = 0.91 - 32.2f_*^2, \tag{19}$$

obtained from a linear fit to data given in Fig. 9. The earlier onset of stagnation of height with frequency is expected to follow this f^2 relation due to the tilt in the effective direction of gravity as discussed in Section 3.2.

4.3. Mass ejection from rotation-induced spreading

Integral to the application of the work presented is the movement of material from the main pile to the edge of the table. This is directly related to the aspect ratio of an initial granular column exceeding a value a_{crit} for a specific frequency such that the runout exceeds a radius r_{crit}.

Percentage mass loss, m_*, was calculated with $0 \le m_* \le 1$ and is plotted against a/a_{crit} in Fig. 10. The value of r_0 does not affect the overall dynamic of the secondary rotation-induced spreading phase, but varies

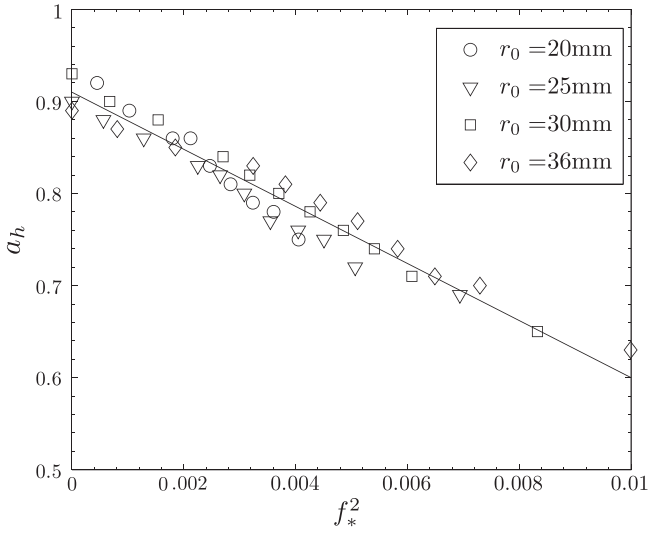

Fig. 9. Onset of stagnating h_f at an aspect ratio a_h against normalised frequency f_*^2. Line fit given by Eq. (19).

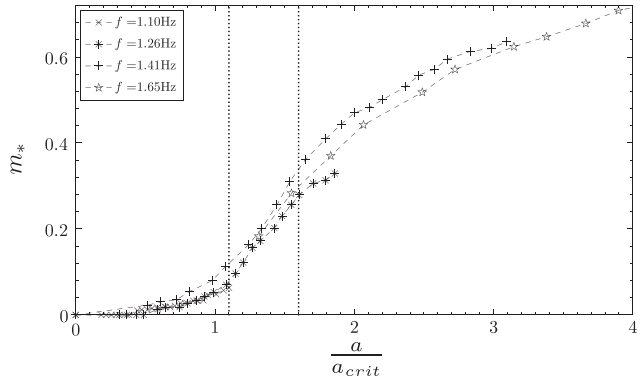

Fig. 10. Mass loss fraction m_* against a/a_{crit} for various frequencies where $r_0 = 36$ mm. Dotted vertical lines indicate a change in the rate of increase of m_*, where it is constant in between them.

the onset as the runout will be different as defined by Eq. (14) in Section 4.1. It can be seen that this follows a logistic shaped curve with a period of acceleration, constant increase and then deceleration.

Mass ejection starts to occur minutely before the final pile radius reaches r_{crit} up to a value of ≈10%. This is seen in Fig. 10 while $\frac{a}{a_{crit}} < 1$ where there is a period of acceleration. The mass loss can be attributed to the collapse itself causing some of the granular matter to saltate and jump from the main frontal flow and exceed the critical radius. While $1.1 < \frac{a}{a_{crit}} < 1.6$ there is a short phase of constant increase in mass loss at approximately the same rate across all frequencies. In this period the mass of the remaining pile continues to increase with height of the granular column, having not reached a saturating value where the pile is stable. Finally a deceleration stage begins where $\frac{a}{a_{crit}} > 1.6$ as the shape of the pile stagnates with any increase in aspect ratio. The additional material at the top of the granular column falls with the frontal flow that exceeds the critical radius and resultantly ejected from the resultant pile.

Theoretically there is no frequency at which the entirety of the mass spreads as the critical radius can never be zero as indicated by the reciprocal relation given in Eq. (10). If you account that the average grain diameter is 700 μm and never sits centrally then every grain will be ejected from the centre at a frequency of approximately 13.5 Hz. It is expected that this would in fact be lower, but was unable to be investigated due to the maximum rotation rate of the equipment.

4.4. Time evolution

To further understand the collapse dynamic, videos of the collapse were taken with a 240 fps camera to study the runout evolution with time. Examples are given in Fig. 11 and where $a = 0.61,\ 1.03$ for $r_0 = 36$ mm. Measurements were made using an alignment grid on the table marked every 10 mm, and a pixel ruler in a photo editing package. Where the rotation is large enough such that the spreading of the granular pile exceeds a radial value r_{crit}, as defined by Eq. 10, the pile achieves a maximal radius r_{max} at a time t_{max}. After this time a period of mass ejection occurs where the radius contracts, settling at a final value $r_f = r_{crit}$. Where material loss occurs, the radius of the runout must be properly defined. This was determined to be the greatest radius where the density of particles still attached to the pile is approximately 1. There was some difficulty in determining this exact radius at times where large amounts of material are being transported from the pile to the edge of the tank, as observed in Fig. 2, with the inaccuracy determined to be ±3 mm.

In the case of no rotation, both aspect ratios exhibit an initial period of acceleration in radial runout then a period of linear growth, followed by a deceleration before settling at a value r_f. Comparing across Fig. 11 **a** and **b**, the length of these individual phases increase with aspect ratio. Considering the increase in frequency of rotation for each aspect ratio,

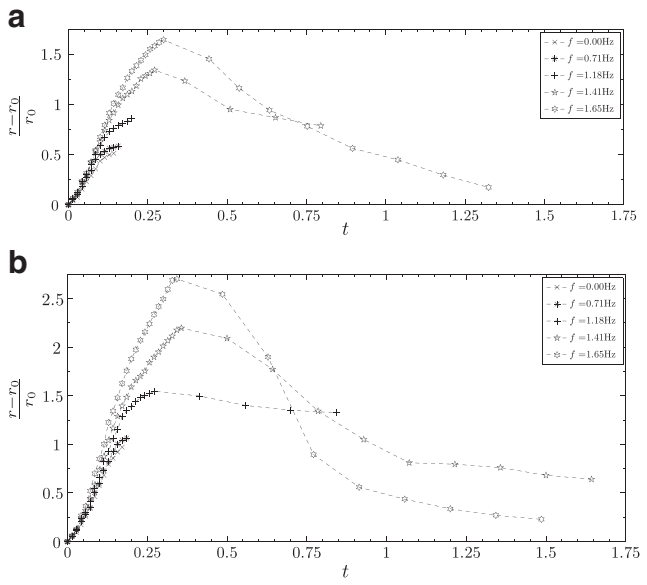

Fig. 11. Evolution of the runout of granular matter for $r_0 = 36$ mm. **a** $a = 0.61$. **b** $a = 1.03$.

the individual phases, speeds of growth and overall collapse time increase. When $f > 1.30$ Hz and $f > 1.18$ Hz for $a = 0.61$ and $a = 1.03$ respectively, after reaching a runout r_{max} at time t_{max} there are additional phases of radial decrease of the main pile when mass is lost from the periphery of the pile during the secondary rotation-induced spreading phase. The onset frequency values correspond to f_{crit} as discussed in Section 4.1 given in Eq. (10). Where this occurs there is a rapid acceleration in the decrease of the radius of the pile before decelerating and settling at a value r_f at time t_f. It is problematic to determine the end of this phase exactly; nearing the end of the period, the radius of the pile may remain essentially static while some material at the periphery of the pile may still eject itself. The error could be as much as ±0.2 s at the highest frequencies, but a smaller error is incurred where the ejection phase is shorter. Determining the total time for collapse where ejection occurs is therefore difficult. In general, for a fixed aspect ratio the acceleration in radial decrease and duration of the phase is greater for increasing frequency. As expected for fixed frequency, the duration of this phase is longer for higher aspect ratios.

The non dimensionlisation of t_f is given by

$$t_* = \frac{t_f}{\sqrt{r_0/g}}. \tag{20}$$

Non-dimensional time was evaluated against aspect ratio for varying frequencies across all cylinder sizes, with an example for $r_0 = 36$ mm given in Fig. 12, revealing

$$t_* = K\sqrt{a} \tag{21}$$

where K is a constant. This was considered for $f < 0.94$ Hz where no mass ejection from the main pile occurred. Considering the proportional constant K against non dimensional frequency f_* for all cylinder radii as in Fig. 13, a linear relationship is evident with

$$K = 18.5 f_* + 3.5. \tag{22}$$

Substituting this into Eq. (21) gives

$$t_* = (18.5 f_* + 3.5)\sqrt{a}. \tag{23}$$

The linearity in f_* is consistent with the effective direction of gravity being tilted due to the introduction of centripetal force and t_* being proportional to $\sqrt{a}$.

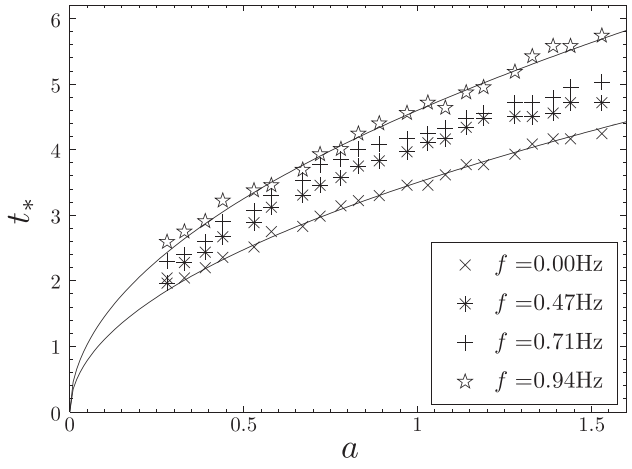

Fig. 12. Normalised total time for collapse against aspect ratio for $r_0 = 36$ mm. Each series follows a $\sqrt{a}$ relation as given in Eq. (21).

For $f > 0.94$ a relation is no longer obvious between non-dimensionalised time and aspect ratio due to the effect of mass ejection increasing the collapse duration. This is compounded with the associated difficulty of realising t_f where even greater mass ejection occurs.

5. Discussion

Granular flows can be difficult to manage theoretically due to the difficulty of relating particle interactions on a small-scale to the macro dynamics of the flow, particularly where solid, fluid and gas phases occur simultaneously. Models of the static arrangement of the rotating granular column collapse configuration discussed here are found from approximation of hydrodynamic equations. The most recent model by Lagrée et al. [24] provides excellent agreement for low to intermediate aspect ratios, but extension of the model to the rotating case requires experimental data prior for verification such as that provided by this study. Given restrictions in current models, it is by the experiments described here that one can draw a comparison to the spreading of granular material as executed by various items of machinery such as road gritters and fertiliser spreaders. Previously observed dimensional scalings [7–9] have been extended to incorporate the effect of rotation, and have uncovered some interesting dynamics.

Under rotation, scalings for the final pile radius followed a similar linear rule to the static case up to the point where the secondary rotation-induced spreading phase occurred, resulting in the stagnation of the final pile radius, found to coincide with the point where the centripetal forces are able to overcome frictional forces. A reversal of this analysis to compare the final pile radius with frequency for fixed aspect ratios revealed the critical radius at which the stagnation occurred for a fixed frequency. Combining this information, a full mathematical description was found for the final radius of the pile in terms of the input parameters r_0, a and f_*. Where there was a maximal runout radius, calculation of the coefficient of friction between the granular material and the tank surface was possible. While this is an empirical result it may find application later in the evaluation of different granular rheologies.

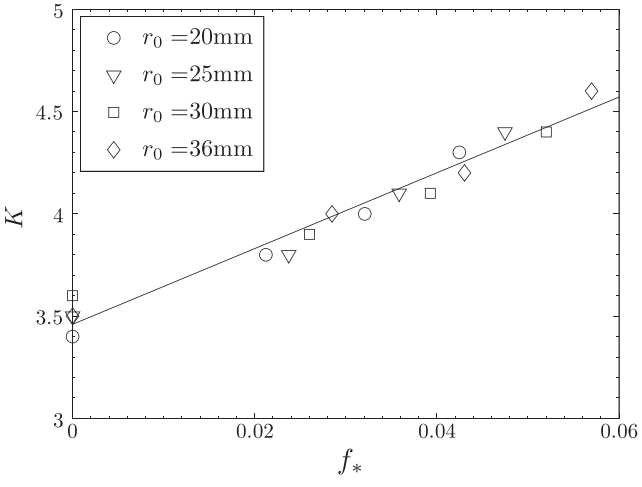

Fig. 13. Dependence of proportional coefficient K given in Eq. (22) on f_*.

The final height of the deposit was less complicated than the radial relation given its stagnating nature and relationship with the effective tilt in gravity caused by the rotation. Together with the radial description, non-dimensional expressions for two defining length scales of the resultant deposit have been found.

The frequency required to initiate mass ejection from the main pile for a set volume of granular material is the main point of interest for industrial applications. It quantifies the minimum amount of rotation to allow spreading of a material and highlights the adjustments that are to be made for different degrees of mass ejection resulting from the secondary rotation-induced spreading of finite volumes of material. Mass loss experiences an initial constant increase where the aspect ratio is large enough that the radial runout exceeds the stagnating value of the final pile radius. This period is short, and the rate of increase begins to decelerate when the aspect ratio is 1.6 times the critical onset.

Differences in runout, height and critical values will exist with different materials and so direct numerical application of scalings found in this study must be used with some care, although the overall dynamics will remain the same. An extension to this work would investigate the spreading of slurries under the same conditions and experimental setup as this would introduce a dependence on shear stresses and shear history.

Appendix A. Supplementary data

Supplementary data to this article can be found online at http://dx.doi.org/10.1016/j.powtec.2014.04.030.

References

[1] P.W. Cleary, M. Prakash, Discrete-element modelling and smooth particle hydrodynamics: potential in the environmental sciences, Philos. Trans. R. Soc. A 362 (2004) 2003–2030.
[2] S.B. Savage, K. Hutter, The dynamics of avalanches of granular material from initiation to runout. Part I: analysis, Acta Mech. 86 (1–4) (1991) 201–223.
[3] Y. Forterre, O. Pouliquen, Granular flows, Sémin. Poincaré 9 (2006) 1–40.
[4] P. Frey, M. Church, Bedload: a granular phenomenon, Earth Surf. Process. Landf. 36 (1) (2011) 58–69.
[5] R.R. Kerswell, Dam break: a model for granular slumping? Phys. Fluids 17 (5) (2005) 057101.
[6] A. Mangeney-Castelnau, F. Bouchut, J.P. Vilotte, E. Lajeunesse, A. Aubertin, M. Pirulli, On the use of Saint Venant equations to simulate the spreading of a granular mass, J. Geophys. Res. 110 (B9) (2005) B09103.
[7] G. Lube, H.E. Huppert, R.S.J. Sparks, M.A. Hallworth, Axisymmetric collapses of granular columns, J. Fluid Mech. 508 (1) (2004) 175–199.
[8] E. Lajeunesse, A. Mangeney-Castelnau, J.P. Vilotte, Spreading of a granular mass on a horizontal plane, Phys. Fluids 16 (2004) 2371–2381.
[9] J.M. Warnett, P. Denissenko, P.J. Thomas, E. Kiraci, M.A. Williams, Scalings of axisymmetric column collapse, Granul. Matter 16 (1) (2014) 115–214.
[10] E.L. Thompson, H.E. Huppert, Granular column collapses: further experimental results, J. Fluid Mech. 575 (2007) 177–186.
[11] P.W. Cleary, M. Frank, Three-dimensional discrete element simulations of axisymmetric collapses of granular columns, Technical Report 44710, Technische Universitat Kaiserslautern, 2006.
[12] G. Lube, H.E. Huppert, R.S.J. Sparks, A. Freundt, Collapses of two-dimensional granular columns, Phys. Rev. E. 72 (4) (2005).
[13] L. Staron, E.J. Hinch, Study of the collapse of granular columns using two-dimensional discrete-grain simulation, J. Fluid Mech. 545 (1) (2005) 1–27.
[14] R. Zenit, Computer simulations of the collapse of a granular column, Phys. Fluids 17 (2005) 031703.
[15] N.J. Balmforth, R.R. Kerswell, Granular collapse in two dimensions, J. Fluid Mech. 538 (2005) 399–428.
[16] S. Siavoshi, A. Kudrolli, Failure of a granular step, Phys. Rev. E. 71 (5) (2005) 051302.

[17] P.V. Liedekerke, E. Tijskens, E. Dintwa, F. Rioual, J. Vangeyte, H. Ramon, DEM simulations of the particle flow on a centrifugal fertilizer spreader, Powder Technol. 190 (3) (2009) 348–360.
[18] F. Rioual, E. Piron, E. Tijskens, Rolling and sliding dynamics in centrifugal spreading, Appl. Phys. Lett. 90 (2) (2007) 021918.
[19] S.Y. Borovikov, L.A. Tarasova, O.A. Troshkin, Movement of a granular material on a rotating disk in a bunker–spreader system, Chem. Pet. Eng. 38 (3) (2002) 124–127.
[20] T. Shinbrot, N.H. Duong, M. Hettenbach, L. Kwan, Coexisting static and flowing regions of a centrifuging granular heap, Granul. Matter 9 (5) (2007) 295–307.
[21] L.P. Kadanoff, Built upon sand: theoretical ideas inspired by granular flows, Rev. Mod. Phys. 71 (1) (1999) 435–443.
[22] S. Douady, B. Andreotti, A. Daerr, On granular surface flow equations, Eur. Phys. J. B 11 (1) (1999) 131–142.
[23] K.P. Hadeler, C. Kuttler, Dynamic models for granular matter, Granul. Matter 2 (1) (1999) 9–18.
[24] P.-Y. Lagrée, L. Staron, S. Popinet, Granular column collapse as a continuum: validity of a two-dimensional Navier–Stokes model with a $\mu(I)$-rheology, J. Fluid Mech. 686 (1) (2011) 378–408.